Precision Measurement of the Electron's Electric Dipole Moment Using Trapped Molecular Ions

William B. Cairncross,[*] Daniel N. Gresh, Matt Grau,[†] Kevin C. Cossel,[‡] Tanya S. Roussy,
Yiqi Ni,[§] Yan Zhou, Jun Ye, and Eric A. Cornell

JILA, NIST and University of Colorado, Boulder, Colorado 80309-0440, USA
and Department of Physics, University of Colorado, Boulder, Colorado 80309-0440, USA
(Received 21 April 2017; published 9 October 2017)

We describe the first precision measurement of the electron's electric dipole moment (d_e) using trapped molecular ions, demonstrating the application of spin interrogation times over 700 ms to achieve high sensitivity and stringent rejection of systematic errors. Through electron spin resonance spectroscopy on $^{180}\text{Hf}^{19}\text{F}^+$ in its metastable $^3\Delta_1$ electronic state, we obtain $d_e = (0.9 \pm 7.7_{\text{stat}} \pm 1.7_{\text{syst}}) \times 10^{-29}$ $e\,$cm, resulting in an upper bound of $|d_e| < 1.3 \times 10^{-28}$ $e\,$cm (90% confidence). Our result provides independent confirmation of the current upper bound of $|d_e| < 9.4 \times 10^{-29}$ $e\,$cm [J. Baron *et al.*, New J. Phys. **19,** 073029 (2017)], and offers the potential to improve on this limit in the near future.

A search for a nonzero permanent electric dipole moment of the electron (eEDM, d_e) constitutes a nearly background-free test for physics beyond the standard model (SM), since the SM predicts $|d_e| \lesssim 10^{-38}$ $e\,$cm [1], while the natural scale of d_e in many proposed SM extensions is 10^{-27}–10^{-30} $e\,$cm [2]. Present experimental results have begun to constrain these theories [3]; hence, there have been many recent efforts to measure an eEDM [3–9].

The most precise eEDM measurements to date were performed using beams of neutral atoms or molecules [3–5]. These experiments benefited from excellent statistical sensitivity provided by a high flux of neutral particles, and decades of past work have produced a thorough understanding of their common sources of systematic error. Nonetheless, a crucial systematics check can be provided by independent measurements conducted using different physical systems and experimental techniques. Moreover, techniques that allow longer interrogation times offer significant potential for sensitivity improvements in eEDM searches and other tests of fundamental physics [10].

In this Letter, we report on a precision measurement of the eEDM using molecular ions confined in a radio frequency (rf) trap, applying the methods proposed in Ref. [11] and demonstrated in Ref. [12]. We perform an electron spin precession experiment on $^{180}\text{Hf}^{19}\text{F}^+$ molecules in their metastable $^3\Delta_1$ electronic state, and extract the relativistically enhanced eEDM-induced energy shift $\sim 2d_e\mathcal{E}_{\text{eff}}$ between stretched Zeeman sublevels, where $\mathcal{E}_{\text{eff}} \approx 23$ GV/cm in HfF$^+$ [13–16]. In addition to leveraging the high eEDM sensitivity and systematic error rejection intrinsic to a $^3\Delta_1$ state in a heavy polar molecule [6,14], we use a unique experimental approach that is robust against sources of systematic error common to other methods. The 2.1(1) s lifetime of the $^3\Delta_1$ state in HfF$^+$

[17] and our use of a rf trap allow us to attain spin precession times in excess of 700 ms—nearly 3 orders of magnitude longer than in contemporary neutral beam experiments. This exceptionally long interrogation time allows us to obtain high eEDM sensitivity despite our lower count rate. In addition, performing an experiment on trapped particles permits the measurement of spin precession fringes at arbitrary free-evolution times, making our experiment relatively immune to systematic errors associated with imperfectly characterized state preparation.

Our apparatus and experimental sequence, shown schematically in Fig. 1, have been described previously [11,12,17–20]. We produce HfF by ablation of Hf metal into a pulsed supersonic expansion of Ar and SF$_6$. The neutral beam enters the rf trap, where HfF is ionized with pulsed UV lasers to form HfF$^+$ in its ground vibronic state [18,19]. The ions are stopped by a pulsed voltage on the radial trap electrodes, then confined by dc and rf electric quadrupole gradients (with $f_{\text{rf}} = 50$ kHz). We next adiabatically turn on a spatially uniform electric bias field $\mathcal{E}_{\text{rot}} \approx 24$ V/cm that rotates in the radial plane of the ion trap with frequency $f_{\text{rot}} \approx 250$ kHz, causing the ions to undergo circular motion with radius $r_{\text{rot}} \approx 0.5$ mm. A pair of magnet coils aligned with the Z axis produces an axial magnetic gradient $\boldsymbol{\mathcal{B}} = \mathcal{B}'_{\text{axgrad}}(2\boldsymbol{Z} - \boldsymbol{X} - \boldsymbol{Y})$ where $|\mathcal{B}'_{\text{axgrad}}| \approx 40$ mG/cm, which in the rotating frame of the ions creates a magnetic bias field $\mathcal{B}_{\text{rot}} \equiv |\langle \boldsymbol{\mathcal{B}} \cdot \mathcal{E}_{\text{rot}}/\mathcal{E}_{\text{rot}} \rangle| \simeq |\mathcal{B}'_{\text{axgrad}} r_{\text{rot}}|$ that is parallel (antiparallel) to $\mathcal{E}_{\text{rot}}$ if $\mathcal{B}'_{\text{axgrad}} > 0$ (<0) [11,12].

Our state preparation consists of population transfer to the eEDM-sensitive $^3\Delta_1$ state and selective depletion of magnetic sublevels to produce a pure spin state [Figs. 1(b) and 1(c)]. Two continuous wave lasers copropagating along the $\hat{Z}$ axis drive a Raman transition through a $^3\Pi_{0^+}$
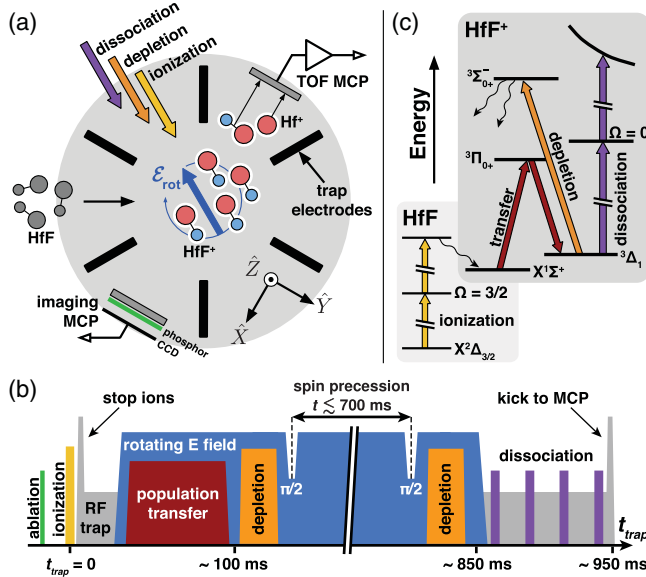
FIG. 1.   (a) Apparatus schematic, (b) experimental timing, and (c) relevant energy levels (not to scale) for an eEDM measurement using trapped ions. HfF is photoionized (yellow) to form HfF$^+$. A rotating electric bias field $\mathcal{E}_{\rm rot}$ (blue) polarizes the molecules, and transfer (red) and depletion (orange) lasers perform state preparation. The $\pi/2$ pulses are performed by modulating $\mathcal{E}_{\rm rot}$. Spin state populations are detected by depletion followed by photodissociation (purple) and counting the resulting Hf$^+$ ions on a microchannel plate (MCP).

intermediate state, transferring $\sim$40% of the ground state population to the $^3\Delta_1$, $J = 1$, $F = 3/2$ state. Figure 2(a) shows the structure of this state in a rotating frame defined by $\mathcal{E}_{\rm rot} \equiv \mathcal{E}_{\rm rot}\hat{z}$. It consists of four Stark doublets (pairs of magnetic sublevels) separated by $d_{\rm mf}\mathcal{E}_{\rm rot}/3h \approx 14$ MHz, where $d_{\rm mf}$ is the $^3\Delta_1$ molecule-frame dipole moment and h is Planck's constant. The population transfer process produces an incoherent mixture of $m_F = \pm 3/2$ states in the upper or lower doublet, depending on the detuning of the second transfer laser. Selective depletion is then performed by a circularly polarized laser resonant with the $Q(1)$ line of a $^3\Sigma_{0^+}^- \leftarrow {}^3\Delta_1$ transition. The depletion laser is strobed synchronously with the rotating electric field so that its wave vector is either parallel or antiparallel to $\mathcal{E}_{\rm rot}$, thus driving a $\sigma^\pm$ transition to an $F' = 3/2$ manifold and leaving one $m_F = \pm 3/2$ level populated in the $^3\Delta_1$ state.

Following strobed depletion, we perform a $\pi/2$ pulse to prepare an equal superposition of $m_F = \pm 3/2$ states. This is accomplished by reducing $\mathcal{E}_{\rm rot}$ for a brief interval, which increases a rotation-induced coupling $\Delta^{u/l}$ between $m_F = \pm 3/2$ states [Fig. 2(b)] and causes a pure spin state to evolve into an equal superposition in $\sim$1 ms [11,12,21]. We return $\mathcal{E}_{\rm rot}$ to its nominal value and allow the phase of the superposition to evolve for a variable precession time, then apply a second $\pi/2$ pulse to map the relative phase of the superposition onto a population difference between $m_F = \pm 3/2$ states. A second set of strobed laser pulses again depletes all but one $m_F = \pm 3/2$ level. To selectively detect
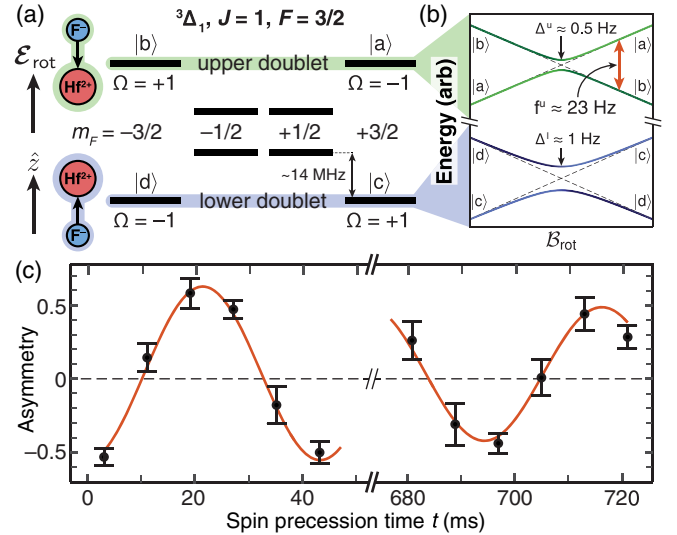

FIG. 2.   Electron spin resonance spectroscopy in HfF$^+$. (a) Level structure of the eEDM-sensitive $^3\Delta_1$, $F = 3/2$ state in an electric bias field $\mathcal{E}_{\rm rot}$. (b) Energies of $|m_F| = 3/2$ states as a function of magnetic bias field $\mathcal{B}_{\rm rot}$ (not to scale), showing an avoided crossing at $\mathcal{B}_{\rm rot} = 0$ due to a rotation-induced coupling $\Delta^{u/l}$ [21]. (c) Interference fringe with interrogation time $\sim$700 ms and decoherence rate $\gamma = 0.3(2)$ s^{-1}.

the remaining population in the $^3\Delta_1$, $J = 1$ state, we resonantly photodissociate HfF$^+$ using pulsed UV lasers [17]. We eject all ions from the trap, and count both Hf$^+$ and the temporally resolved HfF$^+$ using a MCP detector.

We interleave experimental trials where the two sets of strobed depletion pulses have the same or opposite phase with respect to $\mathcal{E}_{\rm rot}$ in order to alternately prepare and detect population in the $m_F = \pm 3/2$ states. Denoting by N_A (N_B) the measured population when the depletion phases are the same (opposite), we form the asymmetry $\mathcal{A} = (N_A - N_B)/(N_A + N_B)$, which normalizes drifts in absolute $^3\Delta_1$ population. The asymmetry forms an interference fringe that is well approximated by a sinusoidal function of precession time t,

$$\mathcal{A}(t) \simeq -\mathcal{C}e^{-\gamma t}\cos(2\pi f t + \phi) + \mathcal{O}, \qquad (1)$$

with frequency f proportional to the energy difference between the $m_F = \pm 3/2$ states, as shown in Fig. 2(c). The initial contrast $\mathcal{C}$, initial phase ϕ, offset $\mathcal{O}$, and decoherence rate γ parametrize imperfect state preparation and the loss of coherence. We perform nonlinear least squares fitting of the asymmetry with Eq. (1), using $\mathcal{C}$, γ, f, ϕ, and $\mathcal{O}$ as fit parameters. Standard errors $\delta\mathcal{C}$, $\delta\gamma$, δf, $\delta\phi$, and $\delta\mathcal{O}$ are estimated from the Jacobian of the fit function at the optimum parameter values. The precession frequency contains the eEDM signal, while the other fit parameters are used to diagnose experimental imperfections and sources of systematic error.

To isolate an eEDM-dependent frequency shift and diagnose systematic errors, we form data "channels":

TABLE I. Selected frequency channels, their leading expression in terms of experimental parameters, and their interpretations. Here δg_{eff} is half the effective magnetic g-factor difference between Stark doublets, α is the tilt angle of $\mathcal{E}_{\text{rot}}$ above the radial plane of the ion trap, and f_{rot} is the rotation frequency of $\mathcal{E}_{\text{rot}}$.

Channel	Leading term	Interpretation
f^0	$3\lvert g_F\rvert\mu_B\mathcal{B}_{\text{rot}}/h$	Avg. precession frequency
f^B	$3\lvert g_F\rvert\mu_B\mathcal{B}_{\text{rot}}^{\text{nr}}/h$	Nonreversing $\mathcal{B}_{\text{rot}}$
f^D	$3\delta g_{\text{eff}}\mu_B\mathcal{B}_{\text{rot}}\text{sgn}(g_F)/h$	Level-dependent g factor
f^{BR}	$-3\langle\alpha\rangle f_{\text{rot}}\text{sgn}(g_F)$	Geometric phase
f^{BD}	$-2d_e\lvert\mathcal{E}_{\text{eff}}\rvert\text{sgn}(g_F)/h$	eEDM shift

FIG. 3. Frequency shifts in the f^B and f^{BR} channels due to a stray uniform magnetic field $\mathcal{B}_Y^{\text{nr}}$ and ion displacements $Y_0\hat{Y}$ and $Z_0\hat{Z}$ [21]. (a) A shift in $f^B \propto \mathcal{B}_Y^{\text{nr}}Y_0$ resulted from a contribution to $\mathcal{B}_{\text{rot}}$ from an electric field gradient oscillating at $2f_{\text{rot}}$, which we suppressed by reducing harmonic distortion in $\mathcal{E}_{\text{rot}}$ via feedforward. (b) A shift in $f^{BR}=3\langle\alpha\rangle f_{\text{rot}} \propto Y_0^2 Z_0$ was well modeled by the known inhomogeneity in $\mathcal{E}_{\text{rot}}$, and was suppressed by applying feedback to the ion position between eEDM measurements. Error bars are $\sim \pm 0.1$ Hz on all points.

components of a measurement that have a particular parity under a set of chosen "switches"—experimental parameters that are modulated between opposite values on a short time scale [27]. Our switches are the sign of the magnetic bias field $\tilde{B}=\text{sgn}(\langle\mathcal{B}\cdot\mathcal{E}_{\text{rot}}\rangle)$, the populated Stark doublet $\tilde{D}=-\text{sgn}(m_F\Omega)$, and the sense of the electric bias field rotation $\tilde{R}=-\text{sgn}(\boldsymbol{\omega}_{\text{rot}}\cdot\hat{Z})$. We repeat our spin precession measurement in each of the eight unique "switch states" $\tilde{S}=(\tilde{B},\tilde{D},\tilde{R})$ to form a "block," and form channels X^s with parities $s\subset\{B,D,R\}$ from linear combinations of the eight measurements $X(\tilde{S})$, where $X\in\{\mathcal{C},\gamma,f,\phi,\mathcal{O}\}$ [see Eq. (S1) in Ref. [21]]. We estimate the standard error δX by propagating the error estimates $\delta X(\tilde{S})$ resulting from the nonlinear least squares fit of Eq. (1).

If higher order effects are neglected, the measured spin precession frequency is dominated by the Zeeman shift between populated magnetic sublevels, and includes a BD-odd contribution from an eEDM,

$$hf(\tilde{S}) \approx \lvert -3g_F\mu_B\tilde{B}\mathcal{B}_{\text{rot}} + 2\tilde{D}d_e\lvert\mathcal{E}_{\text{eff}}\rvert\rvert$$
$$= 3\lvert g_F\rvert\mu_B\mathcal{B}_{\text{rot}} - 2\tilde{B}\tilde{D}\text{sgn}(g_F)d_e\lvert\mathcal{E}_{\text{eff}}\rvert. \quad (2)$$

An eEDM signal thus appears as the lowest-order contribution to the f^{BD} frequency channel, while any nonideal contributions to f^{BD} constitute sources of systematic error. The seven non-eEDM frequency channels contain information about experimental conditions such as nonreversing magnetic fields, and we use these channels to construct and confirm models of nonideal experimental behavior and to correct for systematic shifts in f^{BD}. Some examples of frequency channels, their leading-order expressions in terms of experimental parameters, and their interpretations are shown in Table I.

Prior to eEDM data collection, we tuned a wide variety of experimental parameters over an exaggerated dynamic range and observed the response of the data channels to study nonideal frequency shifts in our system that might affect an eEDM measurement. Two illustrative examples of these effects are shown in Fig. 3, and their contributions to systematics are discussed in Ref. [21]. Through this study, we developed a unified numerical model of our spin
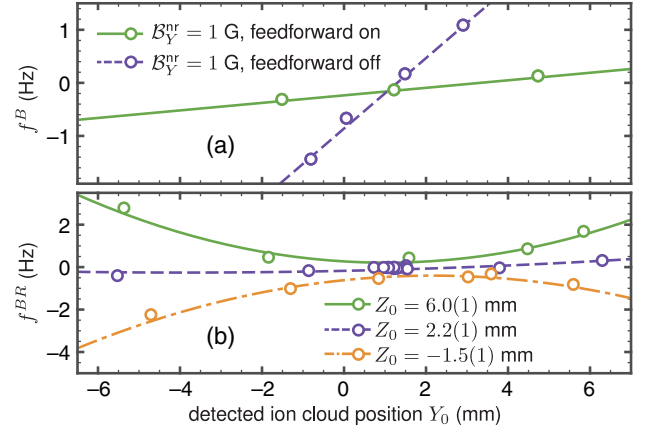
precession sequence. In this model, we integrate the classical motion of ions in simulated time-varying electric and magnetic fields, then propagate the internal quantum state of the molecules using an effective Hamiltonian that includes the two lowest rotational levels of $^3\Delta_1$. Using known experimental parameters and realistic estimates of construction imperfections, our model was able to reproduce all observed frequency shifts.

In total, we collected 1024 blocks (360.3 hours) of eEDM-sensitive data, with each block resulting in one value of f^{BD} and thus one eEDM measurement. Throughout the collection and analysis of this eEDM data, we added to the f^{BD} channel a hidden, computer-generated pseudorandom value drawn from a normal distribution with a standard deviation of 5×10^{-28} e cm. This "blind" allowed us to investigate systematic frequency shifts and perform statistical analysis while mitigating the effects of operator bias. We applied cuts to the blinded data based on non-eEDM channels indicating signal quality: blocks with $\mathcal{C}<0.1$ or $\mathcal{C}e^{-\gamma T}<0.1$ were cut due to low signal to noise (where T is the largest value of t sampled in a block). In addition, we cut data where shifts in the "comagnetometer" channel f^B exceeded 0.4 Hz due to its contribution to systematic errors. After these cuts, our eEDM data set consists of 903 blocks or 313.8 hours of data. The unblinded data set is shown in Figs. 4(a) and 4(b). Normality tests and visual inspection of a normal probability plot indicate that the distribution of normalized and centered eEDM measurements $(f^{BD}-\langle f^{BD}\rangle)/\delta f$ is consistent with a normal distribution. The reduced chi-squared statistic for fitting a weighted mean to the eEDM data set is $\chi_r^2=1.22(5)$. This overscatter is present in all frequency channels, and is attributable to
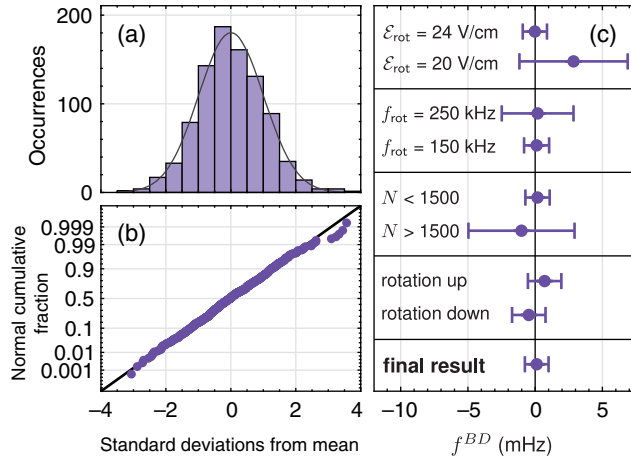
FIG. 4. Summary of eEDM data set after cuts and scaling δf by $\sqrt{\chi_r^2}$ to account for overscatter. (a) Histogram of normalized, centered eEDM-sensitive frequency measurements $(f^{BD} - \langle f^{BD} \rangle)/\delta f$. (b) Normal probability plot of the same data set, showing a linear trend suggesting that the data are consistent with a normal distribution. (c) Subsets of eEDM data taken under different values of experimental parameters, and the overall average of f^{BD}. Here N is the average number of trapped HfF$^+$ ions per run.

nonreversing $\mathcal{B}'_{\text{axgrad}}$ drifts on a time scale comparable to one data block [21]. To compensate for this overscatter, we scale our final statistical error bar by $\sqrt{\chi_r^2} \approx 1.1$.

During eEDM data collection, we suppressed sources of systematic error that appeared in our earlier model-building investigation by applying active feedback to relevant experimental parameters between the collection of data blocks. The only one of these that produced an observable shift in the f^{BD} channel was the combined effect of a nonreversing magnetic bias field $\mathcal{B}_{\text{rot}}^{\text{nr}}$ and the difference in effective magnetic g factor between Stark doublets [11,21]. The f^B and f^D frequency channels, which are acquired concurrently with f^{BD}, provide direct measurements of these contributions. Since the value of $f^D \approx 10^{-3} f^0$ is fixed by the values of $\mathcal{E}_{\text{rot}}$, $\mathcal{B}_{\text{rot}}$, and f_{rot}, we suppress the systematic shift in the eEDM channel by applying a compensating $\mathcal{B}'_{\text{axgrad}}$ to minimize $|f^B|$. We also apply a block-by-block correction to f^{BD} based on the measured values of f^B and f^D, the validity of which was verified in our earlier model-building study [21].

Though they were too small to be observed at our level of sensitivity, we predicted systematic shifts in the eEDM channel due to the frequency shifts in the f^B and f^{BR} channels shown in Fig. 3. We suppressed the first of these by adding a feedforward signal to $\mathcal{E}_{\text{rot}}$ to cancel the harmonic distortion component at $2f_{\text{rot}}$, reducing it from -48 to -70 dBc, and by using magnet coils to null the ambient uniform magnetic field at the rf trap center to within $\sim \pm 30$ mG. To suppress the shift in f^{BR} caused by $\mathcal{E}_{\text{rot}}$ inhomogeneity shown in Fig. 3(b), we measured the ion cloud position once per data block on a pair of MCPs,

TABLE II. Systematic effects and corrections applied to the eEDM channel f^{BD}, in units of μHz [21].

Effect	Correction	Uncertainty
Nonreversing $\mathcal{B}_{\text{rot}}$	-1	5
Geometric phases		4
Axial secular motion		2
Rotation-odd $\mathcal{E}_{\text{rot}}$		14
Doublet population background		195
Total systematic	-1	195
Statistical		868
Total uncertainty		890

and applied dc potentials on the trap electrodes to position the ion cloud within ~ 2 mm of the minimum of the quadratic shift. The residual offset of $f^{BR} \approx -100$ mHz and gradient of $\partial f^{BR}/\partial Y_0 \approx 20$ mHz/mm shown in Fig. 3 are consistent with $\mathcal{E}_{\text{rot}}$ inhomogeneity resulting from realistic machining, welding, and assembly imperfections in the construction of our rf trap.

While collecting eEDM data, we also searched for new systematic errors correlated with parameters that could not be tuned over a significantly exaggerated dynamic range, including $\mathcal{E}_{\text{rot}}$, f_{rot}, and the number of HfF$^+$ ions trapped per experimental trial [Fig. 4(c)]. We did not observe significant variation of f^{BD} with these parameters at our current level of precision. The variations of the non-eEDM frequency channels f^0 and f^D, in which we did anticipate variation with $\mathcal{E}_{\text{rot}}$ and f_{rot}, were consistent with model predictions. Finally, we modified our data collection by randomizing the order of switch states in each block to search for and suppress systematic errors caused by parameter drifts correlated with our switches, and observed no significant variation of data channels [21]. The final results of our systematic error searches and corrections are summarized in Table II.

We removed our blind on 31 March 2017, and obtained a final value for the eEDM-sensitive frequency channel

$$f^{BD} = 0.10 \pm 0.87_{\text{stat}} \pm 0.20_{\text{syst}} \text{ mHz}. \qquad (3)$$

Dividing by $-2|\mathcal{E}_{\text{eff}}|\text{sgn}(g_F)/h \approx 1.13 \times 10^{28}$ mHz/e cm [15,16], we obtain a value for the eEDM,

$$d_e = (0.9 \pm 7.7_{\text{stat}} \pm 1.7_{\text{syst}}) \times 10^{-29} \ e \text{ cm}, \qquad (4)$$

which is consistent with 0 within one standard error. The resulting upper bound is

$$|d_e| < 1.3 \times 10^{-28} \ e \text{ cm} \quad (90\% \text{ confidence}). \qquad (5)$$

Our result is consistent with the limit of $|d_e| < 9.3 \times 10^{-29} \ e$ cm set by the ACME Collaboration [3,28], and we have confirmed their result using a radically different experimental approach. Our measurement is limited by statistics, and our dominant source of systematic

error can be further suppressed to the 10^{-30} e cm level [21]. Here we have assumed that parity and time-reversal violating effects arise purely from d_e. An additional contribution $\sim W_S C_S$ can arise from a pseudoscalar-scalar electron-nucleon coupling C_S [29–32].

Since the completion of this first-generation eEDM measurement, we have constructed a second-generation ion trap that will confine ten times more ions over a one hundred times larger volume, and will provide a larger, more uniform rotating electric bias field. We estimate that these and other improvements should provide an order of magnitude higher eEDM sensitivity. In the further future, we plan to pursue a third-generation eEDM measurement using $^{232}\text{Th}^{19}\text{F}^+$, in which the $^3\Delta_1$ ground electronic state with $\mathcal{E}_{\text{eff}} \approx 36$ GV/cm may allow a coherence time up to tens of seconds [31,33,34].

Note added.—Recently, it came to our attention that the sensitivity coefficient W_S for the pseudoscalar-scalar electron-nucleon coupling has been calculated for HfF$^+$ [35,36].

---

[*]william.cairncross@colorado.edu
[†]Present address: Institute for Quantum Electronics, ETH Zürich, Otto-Stern-Weg 1, 8093 Zürich, Switzerland
[‡]Present address: National Institute of Standards and Technology, 325 Broadway, Boulder, Colorado 80305, USA
[§]Present address: MIT-Harvard Center for Ultracold Atoms, Research Laboratory of Electronics, and Department of Physics, Massachusetts Institute of Technology, Cambridge, Massachusetts 02139, USA

[1] I. B. Khriplovich and M. E. Pospelov, Sov. J. Nucl. Phys. **53**, 638 (1991).
[2] J. Engel, M. J. Ramsey-Musolf, and U. van Kolck, Prog. Part. Nucl. Phys. **71**, 21 (2013).
[3] J. Baron, W. C. Campbell, D. DeMille, J. M. Doyle, G. Gabrielse, Y. V. Gurevich, P. W. Hess, N. R. Hutzler, E. Kirilov, I. Kozyrev, B. R. O'Leary, C. D. Panda, M. F. Parsons, E. S. Petrik, B. N. Spaun, A. C. Vutha, and A. D. West, Science **343**, 269 (2014).
[4] J. J. Hudson, D. M. Kara, I. J. Smallman, B. E. Sauer, M. R. Tarbutt, and E. A. Hinds, Nature (London) **473**, 493 (2011).
[5] B. C. Regan, E. D. Commins, C. J. Schmidt, and D. DeMille, Phys. Rev. Lett. **88**, 071805 (2002).
[6] S. Eckel, P. Hamilton, E. Kirilov, H. W. Smith, and D. DeMille, Phys. Rev. A **87**, 052130 (2013).
[7] K. Zhu, N. Solmeyer, C. Tang, and D. S. Weiss, Phys. Rev. Lett. **111**, 243006 (2013).
[8] B. J. Heidenreich, O. T. Elliott, N. D. Charney, K. A. Virgien, A. W. Bridges, M. A. McKeon, S. K. Peck, D. Krause, J. E. Gordon, L. R. Hunter, and S. K. Lamoreaux, Phys. Rev. Lett. **95**, 253004 (2005).

[9] J. Lee, J. Chen, L. V. Skripnikov, A. N. Petrov, A. V. Titov, N. S. Mosyagin, and A. E. Leanhardt, Phys. Rev. A **87**, 022516 (2013).
[10] L. V. Skripnikov, A. V. Titov, and V. V. Flambaum, Phys. Rev. A **95**, 022512 (2017).
[11] A. E. Leanhardt, J. L. Bohn, H. Loh, P. Maletinsky, E. R. Meyer, L. C. Sinclair, R. P. Stutz, and E. A. Cornell, J. Mol. Spectrosc. **270**, 1 (2011).
[12] H. Loh, K. C. Cossel, M. Grau, K. K. Ni, E. R. Meyer, J. L. Bohn, J. Ye, and E. A. Cornell, Science **342**, 1220 (2013).
[13] Recent high-accuracy calculations yield $\mathcal{E}_{\text{eff}}$ in the range of 22.5–24.2 GV/cm.
[14] E. R. Meyer, J. L. Bohn, and M. P. Deskevich, Phys. Rev. A **73**, 062108 (2006).
[15] A. N. Petrov, N. S. Mosyagin, T. A. Isaev, and A. V. Titov, Phys. Rev. A **76**, 030501 (2007).
[16] T. Fleig and M. K. Nayak, Phys. Rev. A **88**, 032514 (2013).
[17] K.-K. Ni, H. Loh, M. Grau, K. C. Cossel, J. Ye, and E. A. Cornell, J. Mol. Spectrosc. **300**, 12 (2014).
[18] H. Loh, J. Wang, M. Grau, T. S. Yahn, R. W. Field, C. H. Greene, and E. A. Cornell, J. Chem. Phys. **135**, 154308 (2011).
[19] H. Loh, R. P. Stutz, T. S. Yahn, H. Looser, R. W. Field, and E. A. Cornell, J. Mol. Spectrosc. **276–277**, 49 (2012).
[20] K. C. Cossel, D. N. Gresh, L. C. Sinclair, T. Coffey, L. V. Skripnikov, A. N. Petrov, N. S. Mosyagin, A. V. Titov, R. W. Field, E. R. Meyer, E. A. Cornell, and J. Ye, Chem. Phys. Lett. **546**, 1 (2012).
[21] See Supplemental Material at http://link.aps.org/supplemental/10.1103/PhysRevLett.119.153001, which includes Refs. [22–26].
[22] N. R. Hutzler, Ph.D. thesis, Harvard University, 2014.
[23] D. J. Berkeland, J. D. Miller, J. C. Bergquist, W. M. Itano, and D. J. Wineland, J. Appl. Phys. **83**, 5025 (1998).
[24] J. M. Brown and A. Carrington, *Rotational Spectroscopy of Diatomic Molecules* (Cambridge University Press, Cambridge, 2003).
[25] N. J. Stone, At. Data Nucl. Data Tables **90**, 75 (2005).
[26] E. R. Meyer, A. E. Leanhardt, E. A. Cornell, and J. L. Bohn, Phys. Rev. A **80**, 062110 (2009).
[27] Our notation for data channels closely follows that used by the authors of Refs. [3,28].
[28] J. Baron, W. Campbell, D. DeMille, J. Doyle, G. Gabrielse, Y. Gurevich, P. Hess, N. Hutzler, E. Kirilov, I. Kozyrev, B. O'Leary, C. Panda, M. Parsons, B. Spaun, A. Vutha, A. West, and E. West, New J. Phys. **19**, 073029 (2017).
[29] T. Chupp and M. Ramsey-Musolf, Phys. Rev. C **91**, 035502 (2015).
[30] L. V. Skripnikov, J. Chem. Phys. **145**, 214301 (2016).
[31] M. Denis, M. S. Nørby, H. J. A. Jensen, A. S. P. Gomes, M. K. Nayak, S. Knecht, and T. Fleig, New J. Phys. **17**, 043005 (2015).
[32] M. Jung, J. High Energy Phys. 05 (2013) 168.
[33] D. N. Gresh, K. C. Cossel, Y. Zhou, J. Ye, and E. A. Cornell, J. Mol. Spectrosc. **319**, 1 (2016).
[34] L. V. Skripnikov and A. V. Titov, Phys. Rev. A **91**, 042504 (2015).
[35] T. Fleig, arXiv:1706.02893.
[36] L. V. Skripnikov, J. Chem. Phys. **147**, 021101 (2017).